https://doi.org/10.5194/hess-2020-345
Preprint. Discussion started: 21 August 2020


Hydrology and Earth System Sciences
Open Access
Discussions

# Microphysical features of typhoon and non-typhoon rainfall observed in Taiwan, an island in the northwest Pacific.

**Jayalakshmi Janapati[1], Balaji Kumar Seela[1], Pay-Liam Lin[1,2, 3*], Meng-Tze Lee[4], Everette Joseph[5]**

[1]Institute of Atmospheric Physics, Department of Atmospheric Sciences, National Central University, Zhongli district, Taoyuan city, Taiwan

[2]Earthquake-Disaster & Risk Evaluation and Management Center, National Central University, Zhongli district, Taoyuan city, Taiwan.

[3]Research Center for Hazard Mitigation and Prevention, National Central University, Zhongli district, Taoyuan City, Taiwan

[4]Department of Atmospheric and Oceanic Sciences, McGill University, Montreal, Quebec, Canada

[5]National Center for Atmospheric Research, Boulder, Colorado

***Correspondence to:**

Prof. Pay-Liam Lin

Institute of Atmospheric Physics, Department of Atmospheric Sciences

National Central University, Zhongli district, Taoyuan City, Taiwan

Phone: 03-422-3294 03-422-7151 ext. 65509

E-mail: tliam@pblap.atm.ncu.edu.tw

https://doi.org/10.5194/hess-2020-345
Preprint. Discussion started: 21 August 2020


Hydrology and Earth System Sciences
Open Access
Discussions

**Abstract.**

The microphysical features of the typhoon (TY) and non-typhoon (NTY) rainfall in summer seasons are analyzed using long-term (2004 to 2016) data from the impact disdrometer installed in north Taiwan. The RSD stratified based on rainfall rate showed distinct RSD characteristics between TY and NTY rainfall. More (less) number of small (big) size raindrops are noticed in TY rainfall than NTY rainfall. RSD features in terms of gamma parameters are studied for these two weather regimes. The mass-weighted mean diameter ($D_m$) values are higher in NTY than TY rainfall, and an inverse behavior is observed for the normalized intercept parameter ($N_w$). Even after separating the rainfall regimes into convective and stratiform type, a large $D_m$ is found in NTY compared to TY precipitation. Distinct variations in $Z$ –$R$, $D_m$–$R$, $N_w$–$R$, $KE$–$R$, and $KE$–$D_m$ relations are noticed between TY and NTY rainfall. Possible mechanisms responsible for the RSD variations between TY and NTY are discussed using reanalysis, remote-sensing, and ground-based radar datasets.

**Keywords:** typhoon, non-typhoon, disdrometer, rainfall kinetic energy**,** north Taiwan

https://doi.org/10.5194/hess-2020-345
Preprint. Discussion started: 21 August 2020


Hydrology and Earth System Sciences Discussions

## 1. Introduction

Taiwan is an island in the northwest Pacific, with its central mountain range (average height of around 2 km and peaks of ~ 4 km) extending from south to north direction. It is surrounded by the East China Sea in the north, the Philippine Sea in the east, Luzhon strait in the south, and the South China Sea in the southwest. This island is influenced by two major prevailing monsoon regimes: southwesterly monsoon that occur from May to August, and northeasterly monsoon spanning from September to April (Chen and Chen, 2003). Further, rainfall in Taiwan is categorized into winter (December to February), spring (March to April), mei-yu (mid-May to mid-June), summer (mid-June to August), typhoon (May to October), and autumn (September to November) regimes (Chen and Chen, 2003). Among the above mentioned seasons in Taiwan, the summer season is associated with thunderstorm and typhoon weather systems with intense precipitation than the other seasons. Over this island, though there were numerous studies on rainfall characteristics of different weather systems in different seasons (Chen et al., 1999;Chen et al., 2007;Chen et al., 2010;Chen and Chen, 2011;Liang et al., 2017;Tu and Chou, 2013), there are few attempts in elucidating the microphysical aspects of precipitating clouds, especially the raindrop size distribution (RSD).

The RSD offers applications in diverse fields like meteorology, hydrology, remote sensing, and provide an insight into the precipitation microphysics (Rosenfeld and Ulbrich, 2003). The RSD is useful in designing the rainfall estimation algorithms for radar measurements (Ryzhkov and Zrnić, 1995), improving the cloud modeling parameterization (McFarquhar et al., 2015), assessing rainfall erosivity relations (Janapati et al., 2019), validating the remote sensing instruments (Liao et al., 2014;Nakamura and Iguchi, 2007), and in rain attenuation studies (Chen et al., 2011). Owing to RSD applications mentioned above, there were RSD reports for spatial, seasonal (Thompson et al., 2015;Jayalakshmi and Reddy, 2014;Seela et al., 2017;Seela et al., 2018;Krishna et al., 2016) variations, storm to storm, within the storm (Kumari et al., 2014;Maki et al., 2001;Jung et al., 2012), and in different precipitations (Tokay and Short, 1996;Krishna et al., 2016).

There has been an increasing interest in the RSD studies to elucidate the hydrological (Lin and Chen, 2012;Lu et al., 2008;Janapati et al., 2019;Chang et al., 2017), and microphysical characteristics (Chu and Su, 2008;Jung et al., 2012;Seela et al., 2017;Seela et al., 2018;Lee et al., 2019;Janapati et al., 2020) of different precipitating clouds in Taiwan. For instance, Chu and Su (2008) investigated the slope-shape relations for four different precipitations in north Taiwan. In the southern part of Taiwan, the microphysical features of a convective system (a squall line) were investigated by Jung et al. (2012), and they noticed larger $D_m$ values ($N_w$, μ, and Λ) in convective precipitation than the maritime clusters. In north Taiwan, the RSD of thirteen landfall typhoons were reported by Chang et al. (2009). Spatial variations of RSD by Seela et al. (2017) showed that the summer seasons rainfall in Taiwan has more large drops when compared to Palau. They demonstrated that terrain influenced deeply extended convective clouds with more aerosol loading in Taiwan are responsible for the RSD variations between these two islands. Seasonal characteristics of RSD by Seela et al. (2018) established that deep convective clouds in summer and warm clouds in winter seasons resulted in higher $D_m$ values in summer than winter seasons. Microphysics of seasonal rainfall in north Taiwan were analyzed by Lee et al. (2019), and they perceived the highest mean $D_m$ values in the summer and highest concentration ($\log_{10}N_w$) in the winter. Recently, disdrometer observations in Taiwan and India sites showed

https://doi.org/10.5194/hess-2020-345
Preprint. Discussion started: 21 August 2020




higher $D_m$ values in Pacific Ocean tropical cyclones than the Indian Ocean tropical cyclones (Janapati et al., 2020).

There were studies in elucidating the tropical cyclones and non-tropical cyclones RSD characteristics of a given season over India, Australia, China, and Japan (Radhakrishna and Narayana Rao, 2010;Kumar and Reddy, 2013;Deo and Walsh, 2016;Chen et al., 2019;Chen et al., 2017). At a south India station, Gadanki, more small and mid-size drops were observed in tropical cyclonic rainfall than non-cyclonic rainfall (Radhakrishna and Narayana Rao, 2010). At another south India station, Kadapa, more large drops were noticed in northeast monsoon thunderstorm precipitation than the tropical cyclone rainfall (Kumar and Reddy, 2013). In Australia, Deo and Walsh (2016) illustrated the tropical cyclones and non-tropical cyclones RSDs and demonstrated higher $D_m$ values in non-tropical cyclones than tropical cyclones rainfall. The polarimetric radar variables computed with the 2DVD for the typhoon, Mei-yu, and squall line precipitations over Easter China showed distinct differences among these precipitation types (Chen et al., 2017). Over south China, distinct differences in rain integral parameters of typhoons and squall lines were noticed by Zhang et al. (2019). They concluded that it is crucial to adopt the precipitation specific rainfall estimators. Recently, Chen et al. (2019) examined the typhoon and mei-yu rainfall's RSD characteristics and noticed maritime behaviors in the typhoon rainfall and continental behavior in mei-yu rainfall.

Even though there were reports on the rainfall characteristics of the typhoon and non-typhoon rainfall over Taiwan (Chen and Chen, 2011;Tu and Chou, 2013), there is a lack in identifying the RSD features of the typhoon and non-typhoon weather systems associated with

https://doi.org/10.5194/hess-2020-345
Preprint. Discussion started: 21 August 2020


summer seasons over Taiwan. Hence, the current study is motived with the below-mentioned objectives: Do the RSD features of the typhoon and non-typhoon rainfall events in summer seasons for Taiwan show similar or dissimilar characteristics? And if they exist, what are the possible reasons for the RSD differences. Do the typhoon and non-typhoon RSD parameters display comparable/different features to the previous studies? Can we adopt default or tropical rainfall estimation ($Z$–$R$) relations, or do we need to revise them? Henceforth, an attempt is made to study the typhoon and non-typhoon RSD characteristics in summer seasons (16th June to 31st August from 2004 to 2016) at the north Taiwan site.

## 2. Data sets used

The current study utilized the Joss–Waldvogel disdrometer (JWD) (Joss and Waldvogel, 1969) measurements in NCU (24$^{o}$ 58' N, 121$^{o}$ 10' E), Taiwan, from 16 June – 31 August (summer in Taiwan) for 2004 to 2016 years. The summer seasons rainy days in north Taiwan are separated into typhoon (TY) and non-typhoon (NTY) regimes. In identifying the rainfall amounts of typhoons over Taiwan, previous studies adopted different criteria (Tu and Chou, 2013;Chu et al., 2007;Chen et al., 2010). For instance, if a typhoon enters a rectangular box of 21$^{o}$-26$^{o}$ N and 119$^{o}$-125$^{o}$ E, then the corresponding rainfall over Taiwan was considered as typhoon rainfall by Chu et al. (2007). Chen et al. (2010) used a rectangular box of 19.5$^{o}$-27.5$^{o}$ and 117.5$^{o}$-124.5$^{o}$ E to define as the typhoon rainfall when a typhoon invades this box. Similarly, Tu and Chou (2013) used another grid box of 18$^{o}$-29.5$^{o}$ N and 116$^{o}$-126$^{o}$ E to define the typhoon rainfall. In the present study, the rainfall at the disdrometer site is considered as typhoon-induced rain if the typhoons center is $\leq$ 500 km from the disdrometer (Janapati et al., 2019). The rest of the rainy days that were not classified as the typhoon-induced storm were

https://doi.org/10.5194/hess-2020-345
Preprint. Discussion started: 21 August 2020




categorized as non-typhoon rainfall. With this criteria, a total number 59 typhoon, and 131 non-typhoon rainy days were recorded by the JWD in NCU from 2004 to 2016 (excluding 2008 and 2009 years). The geographical location of Taiwan with the disdrometer site (indicated with green color circle) is shown in Fig. 1.

The rain/RSD parameters like raindrop concentration $N(D)$ (mm$^{-1}$ m$^{-3}$), radar reflectivity factor $Z$ (mm$^{6}$ m$^{-3}$), liquid water content $W$ (g m$^{-3}$), rainfall rate $R$ (mm h$^{-1}$), total number concentration $N_t$ (m$^{-3}$), normalized intercept parameter, $N_w$ (m$^{-3}$ mm$^{-1}$), shape parameter $\mu$ (-), and slope parameter $\Lambda$ (mm$^{-1}$), and mass-weighted mean diameter $D_m$ are estimated from the JWD measurements. The formulations for these rain/RSD parameters are detailed in (Seela et al., 2017;Seela et al., 2018;Tokay et al., 2001;Bringi et al., 2003;Tokay and Short, 1996).

In addition to rain parameters, the rainfall kinetic energy (*KE*) that is expressed in *KE* flux ($KE_{time}$, in J m$^{-2}$ h$^{-1}$) and *KE* content ($KE_{mm}$, J m$^{-2}$ mm$^{-1}$) are computed for TY and NTY rainy days of summer seasons for north Taiwan by following the procedures of (Fornis et al., 2005;Salles et al., 2002;van Dijk et al., 2002).

Along with the disdrometer data, remote-sensing (TRMM and MODIS) and reanalysis (ERA-interim) data sets are used to elucidate the typhoon and non-typhoon rainy days' microphysical characteristics. Bright band and storm heights from TRMM satellite data product (2A23)(Iguchi et al., 2000;Kummerow et al., 2001), Cloud effective radii of liquid and ice particles from MODIS satellite data product (MOD08_D3) (Platnick et al., 2015;Remer et al., 2005;Nakajima and King, 1989), water vapor, convective available potential energy, relative

https://doi.org/10.5194/hess-2020-345
Preprint. Discussion started: 21 August 2020




humidity and temperature profiles from ERA-Interim (Dee et al., 2011) are considered for TY and NTY rainy days. Both remote-sensing and reanalysis data sets are interpolated to 0.125° × 0.125° over the disdrometer site. A brief description of these data sets can be found in (Seela et al., 2018;Janapati et al., 2020).

Besides remote-sensing and re-analysis data sets, the radar reflectivity profiles from radars mosaic are used to reveal the rainfall characteristics of TY and NTY rainy days. The Z profiles are obtained from the six radars that are depicted with red triangles in Fig. 1. The Z profiles for the period of 2005-2014 are used over the observational sites, and an explanation of the reflectivity profiles from six ground-based radars is provided in Seela et al. (2018).

## 3. Observational Results

The disdrometer rainy days, which have nearly equal amounts of rainfall to that of the collocated rain gauge observations (data points in Fig. 2), are used to demonstrate the raindrop size distribution (RSD) features of the typhoon (TY) and non-typhoon (NTY) rainfall. The JWD recorded a total of 23074 and 20368 rainy minutes for TY and NTY precipitations. The mean raindrop concentrations for TY and NTY rainfalls are provided in Fig. 3a. Throughout this paper, raindrops of diameter greater than 3 mm, 1−3 mm, and less than 1 mm are named, respectively, as large, mid, and small size drops (Tokay et al., 2008;Seela et al., 2018). From Fig. 3a, it can be noticed that the NTY rainy days have more large size drops than the TY rainy days. A clear separation between TY and NTY rainfall RSD can be noticed. Because of drop concentrations dependency on the rainfall rate, it is difficult to interpret the RSD difference between TY and NTY rainfall from Fig. 3a. Hence we adopted the normalization (Testud et al., 2001) to the TY and NTY rainy days RSD. This method is independent of the shape of the observed raindrop spectra. It can be useful in comparing the RSD of different precipitations and inspecting them for indications of differences in the physical processes producing the rain. The drop diameter (*D*, mm), raindrop concentrations [*N(D)*, $mm^{-1}$ $m^{-3}$] of TY and NTY precipitations are normalized by mass-weighted mean diameter ($D_m$, mm) and normalized intercept parameter ($N_w$, $mm^{-1}$ $m^{-3}$), respectively, and are shown in Fig. 3b. From the figure, it is apparent that the normalized NTY spectra depart noticeably from the TY spectra for $D/D_m > 2$, suggesting that the rain production in TY and NTY is involved with substantially different microphysical processes.

The probability distribution functions (PDF) of $D_m$ (mass-weighted mean diameter in mm), $\log_{10}N_w$ ($N_w$ is normalized intercept parameter in $mm^{-1}$ $m^{-3}$), $\log_{10}R$ (*R* is rainfall rate in mm $h^{-1}$), and $\log_{10}W$ (*W* is the liquid water content in g $m^{-3}$), for TY and NTY rainy days, are depicted in Fig. 4. The PDF distributions of $D_m$ in TY and NTY rainy days clearly show that NTY rainy days have higher distributions than TY rainy days for $D_m$ values great than 1.7 mm (Fig. 4a). The normalized intercept parameter,$\log_{10}N_w$ ($\underline{N_w}$ in $m^{-3}$ $mm^{-1}$) PDF distributions show peak values around 3.7 $m^{-3}$ $mm^{-1}$ and 3.4 $m^{-3}$ $mm^{-1}$, respectively, for TY and NTY rainy days (Fig. 4b). The TY and NTY rainy days have peak PDF distributions of $\log_{10}R$ around 0.3 and 0, respectively (Fig.4c). The PDF of $\log_{10}W$ shows a higher percentage at lower $\log_{10}W$ values ($\log_{10}W < -1$) in NTY rainy days, and a higher percentage at higher $\log_{10}W$ values ($\log_{10}W > -1$) in TY rainy days (Fig. 4d). Further, a statistical (Student's t-test) test performed for parameters in Fig. 4 showed that the results rejected the null hypothesis at significance levels of 0.05 and 0.01.

https://doi.org/10.5194/hess-2020-345
Preprint. Discussion started: 21 August 2020




### 3.1 Contribution of raindrop diameters to $N_t$ and $R$

The contribution of raindrop diameter classes (diameter < 1 mm, 1−2 mm, 2−3 mm, 3−4 mm, and 4−5 mm) to $N_t$ ($m^{-3}$) and $R$ (mm $h^{-1}$) for TY and NTY rainy days are shown in Fig. 5. From Fig.5a & b, it can be seen that for both TY and NTY rainy days, with the increase of drop diameter classes, contribution to total number concentration decreased, while that of rainfall rate increased and then decreased. This characteristic also agrees with the findings of previous studies on tropical cyclones (Chen et al., 2019) and summer season rainfall (Wu et al., 2019). For both TY and NTY rainy days, small size drops (< 1 mm) predominantly contributed to a large number concentration (> 70%) and about 10% to rainfall rate. Raindrops with diameter 1−2 mm contributed to number concentration around 20% for TY and NTY rainy days and to rainfall rate around 60% (55%) for TY (NTY) rainy days. The contribution of drops with diameters 2−3 mm to number concentration is negligible (for both TY and NTY days), and the rainfall rate is above 20% for TY and NTY rainy days. Fig. 5a and b clearly emphasize that small (< 1 mm) and mid-size drops (1−3 mm) contributed to a higher percentage of total number concentration and rainfall rate.

The ratio of $N_t$ ($m^{-3}$) occurrence in TY and NTY rainy day to the both (TY+NTY) rainy days in each drop diameter class are illustrated in Fig.5c. Similarly, the ratio of $R$ (mm $h^{-1}$) occurrence in TY and NTY rainy day to the both (TY+NTY) rainy days in each drop diameter class are illustrated in Fig.5d. The percentage of $N_t$ ($m^{-3}$) in the first three drop diameter classes (< 1 mm, 1−2 mm, 2−3 mm), i.e., for the small and mid-size drop classes, is higher in TY than NTY rainy days. On the other hand, for the raindrop diameter classes greater than 3 mm, the occurrence percentage of $N_t$ ($m^{-3}$) is higher in NTY than TY rainy days. Similar to the $N_t$ ($m^{-3}$),

https://doi.org/10.5194/hess-2020-345
Preprint. Discussion started: 21 August 2020



the percentage of rainfall rate is higher in TY than NTY rainy days for small and mid-size drops, and an opposite feature can be seen for large drops (> 3 mm).

### 3.2 Segregation of RSD based on rainfall rates

The total RSDs of TY and NTY rainfall are stratified into seven rainfall rate classes. These rainfall rate classes are considered with the below-mentioned conditions. There were sufficient data points in every class for TY and NTY rainy days, and the mean values of rainfall rates in each category are nearly equal. A similar classification criterion was assumed by (Jayalakshmi and Reddy, 2014;Deo and Walsh, 2016;Seela et al., 2017). Statistical values of these seven rainfall rate classes in TY and NTY rainy days are given in Table 1. Each rainfall rate class's mean value is nearly equal in TY and NTY rainy days. Except for fourth and fifth rainfall rate classes (C4 and C5), the skewness is higher in NTY than TY rainy days, and both the weather systems (TY, NTY) showed +ve skewness, which indicates that the rainfall rates are focused on the left to the mean.

Following the procedure mentioned in Seela et al. (2018), the RSD variations between TY and NTY rainfall in seven rainfall rate classes are evaluated in terms of drop concentration percentage and are illustrated in Fig. 6. The drop-concentration percentage is the ratio of $N(D)$ in TY or NTY rainy days for the raindrop diameter $D$ and rainfall rate class $R$ to the raindrop concentration accumulations in TY and NTY rainy days. The percentage contribution of $N(D)$ for TY and NTY rainy days demonstrates that, for all the rainfall rate classes, the small and mid-size drops (< 3 mm) have a higher percentage in TY than NTY rainy days. Whereas, the large drops (> 3 mm) show a higher percentage of $N(D)$ for NTY than TY rainy days.

https://doi.org/10.5194/hess-2020-345
Preprint. Discussion started: 21 August 2020



Distributions of $D_m$ (mm) and $\log_{10}N_w$ ($m^{-3}$ $mm^{-1}$) for seven rainfall rate classes are depicted with box plots in Fig. 7. From Fig. 7a, it is evident that with rainfall rate class increase, an increase in $D_m$ values can be seen for both TY and NTY rainy days, which is due to a raise in large size drops concentration and a reduction in the concentration of small drops with the rainfall rates increase (Rosenfeld and Ulbrich, 2003;Krishna et al., 2016). On the other hand, $D_m$ values are higher in NTY than TY rainy days in all the rainfall rate classes due to the more concentration of mid-size and small size raindrops in TY than NTY rainy days (Fig.6). Compared to $D_m$, for all seven rainfall rate classes, the $\log_{10}N_w$ values are higher in TY than NTY rainy days (Fig.7b).

Distributions of $D_o$ [$D_o = (3.67+ \mu)/\Lambda$] and $\log_{10}N_w$ in different rainfall rates classes (< 5, 5−10, 10−30, 30−50, and > 50 mm $h^{-1}$) for TY and NTY rainy days are illustrated in Fig. 8a & b. The stratiform and convective classification lines of Thompson et al. (2015) and Bringi et al. (2009) are denoted, respectively, with horizontal black dotted and slant solid lines. With the rainfall rate classes increase, the distributions $D_o$, and $\log_{10}N_w$ are getting narrowed for both TY and NTY rainy days. The $D_o$ and $\log_{10}N_w$ data points were distributed in convective and stratiform regions of Bringi et al. (2009) precipitation classifications line (inclined solid line in Fig. 8) for rainfall rates > 10 mm $h^{-1}$ and < 10 mm $h^{-1}$, respectively. Mean values of $D_o$ and $\log_{10}N_w$ in different rainfall rates for TY and NTY rainy days are depicted in Fig. 8c & d. For both TY and NTY rainy days, mean $D_o$ values increase with the increase of $R$ classes. Moreover, for $R$ > 10 mm $h^{-1}$, mean $D_o$, and $\log_{10}N_w$ values were distributed in the convective region of Bringi et al. (2009) classification line (Fig. 8c & d). Further, the TY rainy days mean $\log_{10}N_w$ values are found to be equal or very slightly higher than the Thompson et al. (2015) rainfall classification line for rainfall rates > 10 mm $h^{-1}$ (Fig. 8c). On the other hand, for all rainfall rate classes, the NTY rainy days, mean $\log_{10}N_w$ values are smaller than the rain classification line of Thompson et al. (2015) (Fig.8d). This shows that, in separating the TY and NTY rainy days of summer seasons over north Taiwan into stratiform and convective type, Bringi et al. (2009) classification method is superior to that of the Thompson et al. (2015).

## 3.3 RSDs in precipitation types

The RSDs were found to show distinct features with the precipitation types, and there were numerous reports in separating the precipitations into stratiform and convective types (Ma et al., 2019;Jayalakshmi and Reddy, 2014;Ulbrich and Atlas, 2007). For instance, Tokay and Short (1996) reported variations in convective precipitations to that of the stratiform regimes. There were reports in emphasizing to adopt precipitation specific rainfall estimation relations (Ulbrich and Atlas, 2007). In this work, TY and NTY rainfall are segregated to convective and stratiform regimes using the rain classification method detailed in Ma et al. (2019). Distributions of mean $N(D)$ ($m^{-3}$ $mm^{-1}$) with raindrop diameters for TY and NTY rainy days in two precipitation regimes are depicted in Fig. 9a. The drop concentration of the convective rainfall is higher than the stratiform for all the drop diameters except for the first drop size bin. Concave shape with broader distributions of $N(D)$ in convective than stratiform is due to the breakup of large drops by collisions (Hu and Srivastava, 1995). Present RSD features in both precipitation types are similar to the earlier studies for continental (Jayalakshmi and Reddy, 2014) and oceanic regions (Krishna et al., 2016). On the other hand, in stratiform and convective regimes, the mid-size and large drops concentration is higher in NTY than TY rainy days. Variations in $D_m$ and $\log_{10}N_w$ for both precipitations of TY and NTY are depicted in Figure 9b. The maritime and continental convective clusters of Bringi et al. (2003) are depicted with gray rectangles. For both TY and NTY rainy days, larger mean $D_m$ and $\log_{10}N_w$ can be seen for convective precipitation. In contrast to that, in stratiform and convective regimes, the NTY rainy days have smaller $\log_{10}N_w$ and larger $D_m$ values than TY rainy days.

### 3.4 Rainfall estimation relations

Usage of the $Z-R$ relations that are region, weather system, and precipitation specific can minimize the weather radars' rainfall estimation uncertainties. In $Z = A R^b$ relation, The drop size can be inferred from the coefficient 'A', and the microphysics from exponent 'b'(Atlas et al., 1999;Steiner et al., 2004;Atlas and Williams, 2003). The TY and NTY rainfall $Z-R$ relations derived from the linear regression applied to 10*log10$R$, and $Z$, and are provided in Fig. 10. The coefficient values of $Z-R$ relations are larger in NTY than the TY for stratiform and convective precipitations, as well as for total rainfall. This variation is due the presence of significant number of large size drops in NTY to that of the TY rainfall. Moreover, the obtained TY and NTY rainy days $Z-R$ relations are found to be varying from the default ($Z=300 R^{1.4}$) and tropical $Z-R$ relationships ($Z=250R^{1.2}$), which suggests adopting the weather and region-specific $Z-R$ relations.

### 3.5 The rainfall rate relationships with $D_m$ and $N_w$

The normalized intercept parameter and mass-weighted mean diameter can provide the RSD features, and these parameters were found to show uniqueness with the rainfall rate (Chen et al., 2016;Janapati et al., 2020). Scatter plots of $D_m$ and $\log_{10}N_w$ versus $R$ for TY and NTY rainy days are depicted in Fig. 11. For both TY and NTY rainy days, with an increase in rainfall

https://doi.org/10.5194/hess-2020-345
Preprint. Discussion started: 21 August 2020

Hydrology and Earth System Sciences
Discussions

rates, the distributions of $D_m$ get narrowed. Similar behavior was reported in previous studies on tropical cyclone and summer season rainfall (Kumar and Reddy, 2013;Wen et al., 2018;Chang et al., 2009;Janapati et al., 2020;Chen et al., 2019;Wu et al., 2019). For both TY and NTY rainy days, fewer variations in $D_m$ values for $R$ > 25 mm h$^{-1}$ is due to the reaching of RSD to equilibrium condition through raindrop breakup and coalescence, (Hu and Srivastava, 1995), and an increase in number concentration can lead to a further increase in rainfall rates (Bringi and Chandrasekar, 2001). The non-linear least-squares fitting equations for $D_m$ versus $R$, and $\log_{10}N_w$ versus $R$ are given in Fig. 11. The $D_m$–$R$ relations depicts that the NTY rainy days have a relatively higher coefficient value than TY rainy days, and the coefficient value of $N_w$–$R$ relations is higher in TY than NTY rainy days. This feature confirms that the NTY rainy days have higher $D_m$ and lower $N_w$ values for given rainfall rates than the TY rainy days.

### 3.6 *KE–R and KE–$D_m$* relations

The raindrops falling from the cloud base reach the ground with a certain amount of kinetic energy (*KE*), and they can erode the soil from the ground surface. Hence, the raindrops *KE* or rainfall *KE* is one of the critical physical quantities in soil erosion studies (Wischmeier, 1959;Kinnell, 1981). As the rainfall *KE* is related to the raindrop diameter and its fall velocity, it can be evaluated through the RSD information (Kinnell, 1981). The empirical relations between the rainfall *KE* and rainfall intensity are incorporated in assessing the rainfall erosivity factor (R-factor) that is used in soil erosion modeling studies (Renard et al., 1997;Janapati et al., 2019). In this section, empirical relations between the rainfall *KE* ($KE_{time}$ in J m$^{-2}$ h$^{-1}$; $KE_{mm}$ in J m$^{-2}$ mm$^{-1}$) and rainfall rate (mm h$^{-1}$) are derived using non-linear least-squares regression method for both TY and NTY rainy days. The distribution plots of $KE_{mm}$ and $KE_{time}$ with $R$ for TY and

NTY rainy days are portrayed in Fig. 12. The $KE_{time}$–$R$ empirical relations are derived by fitting the data points with power and liner methods. For both TY and NTY rainy days, the power-law line fitted well by passing through the middle of the data points at both lower and higher rainfall rates than the linear fit line (Fig. 12a & b). The $KE_{mm}$ and $R$ data points are fitted with power, logarithmic, and exponential law. Among three forms of relations, the power-law fitted well with the data points for both TY and NTY rainy days (Fig. 12c &d). Moreover, empirical relations between $D_m$ (mm), the $KE_{mm}$ are evaluated for both TY and NTY rainy and are given in Fig. 13. Comparison of present $KE$−$D_m$ relations with the East China seasonal rainfall $KE$−$D_m$ ($KE$ = $-2.33D_m^2 + 21.05D_m - 7.79$) relation showed that both TY and NTY relations in Taiwan are different from that of East China (Wen et al., 2019). The derived $KE$−$D_m$ relations can be used to estimate the $KE$ values from the remote-sensing radar (GPM DPR) measurements. The $KE_{time}$–$R$, $KE_{mm}$–$R$, and $KE$−$D_m$ relations and their statistical values are given in Table 2. For both $KE_{time}$–$R$, $KE_{mm}$–$R$ relations, the power-law showed higher CC and lower RMSE and NRMSE values, suggesting to adopt the power form equation to estimate the rainfall $KE$.

## 4. Discussion

To understand the possible mechanisms responsible for the RSD distinctions between TY and NTY rainy days, re-analysis, remote sensing, and ground-based radar data sets are used. The water vapor and CAPE values for TY and NTY rainy days over the disdrometer measurement site are depicted with a box plot in Fig. 14. The water vapor and CAPE values are more significant in NTY than TY rainy days, suggesting that NTY rainfall events have severe convective activity with vigorous updrafts and downdrafts than TY rainy days. However, if we look at the storm and bright band heights (BBH) (Fig. 15), TY rainfall events have relatively higher BBH than NTY rainy days, and there is no much difference in storm heights between TY and NTY rainy days. The ice and liquid particles cloud effective radii are illustrated in Fig. 16. Relatively higher BBH in TY supports the higher CER values of ice particles in TY than NTY rainy days (Fig. 16b). On the other hand, there is no much difference in the CER values of the liquid particle between TY and NTY rainy days (Fig.16a). The deep stratiform clouds in TY rainy days offer sufficient time to the ice crystals to grow larger size (via aggregation and vapor deposition). They yield raindrops of large size after the passage of the melting layer. Because of the relatively higher BBH in TY rainfall events, below to the melting layer, the equilibrium RSD will be achieved through the different microphysical processes (collision, coalescence, and breakup) in TY than NTY rainfall days (Hu and Srivastava, 1995). In contrast, higher convective activity in NTY rainy days proposes that the RSD in these intense clouds varies by enhancing the collision-coalescence process and drop sorting. It allows the smaller drops to shoot to higher altitudes through resilient updraft and allowing large drops to reach the surface. The relative humidity and air temperature profiles are portrayed in Fig. 17. The profile of air temperature shows no much variation between TY and NTY rainy days (Fig.17a). On the other hand, relative humidity vertical profile values are higher in TY than NTY rainfall, suggesting that the NTY rainy days were associated with relatively drier conditions than TY days. The rate of evaporation of small drops produced through the collision breakup processes in NTY is higher than TY rainy days resulting in more large drops in NTY rainy days.

The radar reflectivity CFAD (contoured frequency-by-altitude diagrams) for (a) typhoon (TY) and (b) non-typhoon (NTY) rainy days of summer seasons are given in Fig. 18. The horizontal dotted lines in Fig.18 are the freezing level heights that are computed from the

https://doi.org/10.5194/hess-2020-345
Preprint. Discussion started: 21 August 2020


Hydrology and Earth System Sciences
Discussions

radiosonde data from Banqiao (121.441°E, 24.997°N) and Hualien (121.619°E, 23.989°N) stations. The horizontal sky blue (dark magenta) dotted line in Fig.18a (Fig.18b) is melting layer height mean of TY (NTY) rainy days, and the white dotted line is the mean of both TY and NTY melting layer heights. The vertical sky blue (dark magenta) star line in Fig. 18a (Fig.18b) is the mean radar reflectivity profile of TY (NTY) rainy days. The white-star dotted profile in Fig.18a & b is the mean of both TY and NTY rainy days' reflectivity profiles. The mean reflectivity profile of TY (NTY) rainy days is less (higher) than the mean of TY and NTY rainy days' reflectivity profile. A higher occurrence percentage of lower $Z$ values ($Z$ < 10 dBZ) in TY than NTY rainy days can be seen at higher altitudes. In contrast to that, below the melting layer, the occurrence percentage of higher reflectivity values is ($Z$ > 40 dBZ) is higher in NTY than TY rainy days. The mean vertical profiles of radar reflectivity for TY and NTY rainy days are plotted in Fig. 19. It can be seen that the mean reflectivity values are higher in NTY than TY rainy days. As the radar reflectivity is directly related to the raindrop diameter of power six, from the reflectivity profiles, it can be inferred that bigger drops are predominant in NTY than TY rainy days. Those mentioned above thermodynamical and microphysical processes resulted in more big size drops and few small drops in NTY than TY rainy days, resulting in higher $D_m$ and lower $N_w$ values in NTY than TY rainy days.

## 5. Summary and conclusions

The summer seasons typhoon (TY) and non-typhoon (NTY) rainy days raindrop size distributions (RSD) are investigated using long-term (2004-2016) ground-based disdrometer measurements that were measured in north Taiwan. In addition to disdrometer, remote-sensing, re-analysis, and ground-based radar data sets are used to elucidate the feasible mechanism

https://doi.org/10.5194/hess-2020-345
Preprint. Discussion started: 21 August 2020

Hydrology and Earth System Sciences
Open Access
EGU
Discussions

responsible for RSD distinctions in TY and NTY rainfall. The NTY rainy days of summer seasons have more big size drops and fewer small size drops than the TY rainy days. The classification of RSD to varying rainfall rates and precipitation regimes clearly showed larger $D_m$ values and smaller $N_w$ values in NTY than TY rainy days. The $Z-R$, $D_m-R$, $N_w-R$, $KE_{time}-R$, $KE_{mm}-R$, and $KE_{mm}-D_m$ relations were different for TY and NTY rainfall. Relatively higher convective activity with drier conditions in NTY than TY rainy days resulted in distinct RSD features between these two weather systems. The results detailed in this study could help in evaluating the radar precipitation estimation algorithms, cloud modeling, and rainfall erosivity studies.

*Data availability.* The Era-interim re-analysis data can be obtained from https://www.ecmwf.int/en/forecasts/datasets/reanalysis-datasets/era-interim. The TRMM data can be retrieved from https://gpm.nasa.gov/data/directory. The MODIS cloud data product can be accessed through https://modis.gsfc.nasa.gov/data/dataprod/mod06.php. The ground-based radar and disdrometer data are available from the corresponding author upon reasonable request.

*Author contributions.* JJ and BKS conceptualized the idea; PLL and EJ provided funding acquisition, project administration, and observation data; JJ, BKS, and MTL conducted the detailed analysis; PLL, and EJ supervised the analysis; JJ, BKS wrote the initial manuscript; JJ, BKS, PLL reviewed and revised the manuscript; all authors involved in writing the manuscript and revisions.

*Competing interests.* No conflict of interest is declared by the all authors.

*Acknowledgements*. We acknowledge the Central Weather Bureau (CWB) of Taiwan, in facilitating the radar reflectivity data, and Tropical Rainfall Measuring Mission (TRMM), ERA-Interim and MODIS research team for their efforts in providing the data. This research work is carried out under the Taiwan Ministry of Science and Technology (MOST) grant numbers: MOST 108-2111-M-008-028, MOST 108-2625-M-008-011, MOST: 104-2923-M-008-003 and partially by "Earthquake-Disaster & Risk Evaluation and Management Center, E-DREaM" from The Featured Areas Research Center Program within the framework of the Higher Education Sprout Project by the Ministry of Education (MOE), Taiwan. The first author, JJ is supported by the grant number MOST 108–2811–M–008–558, and second author, BKS, by MOST 108-2625-M-008-011 and MOST 108-2811-M-008-595.

https://doi.org/10.5194/hess-2020-345
Preprint. Discussion started: 21 August 2020


Hydrology and Earth System Sciences
Discussions

# References


Atlas, D., Ulbrich, C. W., Marks Jr, F. D., Amitai, E., and Williams, C. R.: Systematic variation of drop size and radar-rainfall relations, Journal of Geophysical Research: Atmospheres, 104, 6155-6169, 10.1029/1998JD200098, 1999.

Atlas, D., and Williams, C. R.: The Anatomy of a Continental Tropical Convective Storm, Journal of the Atmospheric Sciences, 60, 3-15, 10.1175/1520-0469(2003)060<0003:Taoact>2.0.Co;2, 2003.

Bringi, V., Williams, C., Thurai, M., and May, P.: Using dual-polarized radar and dual-frequency profiler for DSD characterization: A case study from Darwin, Australia, Journal of Atmospheric and Oceanic Technology, 26, 2107-2122, 2009.

Bringi, V. N., and Chandrasekar, V.: Polarimetric Doppler Weather Radar: Principles and Applications, Cambridge University Press., 2001.

Bringi, V. N., Chandrasekar, V., Hubbert, J., Gorgucci, E., Randeu, W. L., and Schoenhuber, M.: Raindrop Size Distribution in Different Climatic Regimes from Disdrometer and Dual-Polarized Radar Analysis, Journal of the Atmospheric Sciences, 60, 354-365, 10.1175/1520-0469(2003)060<0354:RSDIDC>2.0.CO;2, 2003.

Chang, J. M., Chen, H. E., Jou, B. J. D., Tsou, N. C., and Lin, G. W.: Characteristics of Rainfall Intensity, Duration, and Kinetic Energy for Landslide Triggering in Taiwan, Engineering Geology, 231, 81-87, 10.1016/j.enggeo.2017.10.006, 2017.

Chang, W.-Y., Wang, T.-C. C., and Lin, P.-L.: Characteristics of the Raindrop Size Distribution and Drop Shape Relation in Typhoon Systems in the Western Pacific from the 2D Video Disdrometer and NCU C-Band Polarimetric Radar, Journal of Atmospheric and Oceanic Technology, 26, 1973-1993, 10.1175/2009jtecha1236.1, 2009.

Chen, B., Wang, J., and Gong, D.: Raindrop size distribution in a midlatitude continental squall line measured by thies optical disdrometers over East China, J. Appl. Meteor. Climatol., 55, 621–634, 10.1175/JAMC-D-15-0127.1, 2016.

Chen, C.-S., and Chen, Y.-L.: The Rainfall Characteristics of Taiwan, Monthly Weather Review, 131, 1323-1341, 10.1175/1520-0493(2003)131<1323:TRCOT>2.0.CO;2, 2003.

Chen, C.-S., Chen, Y.-L., Liu, C.-L., Lin, P.-L., and Chen, W.-C.: Statistics of Heavy Rainfall Occurrences in Taiwan, Weather and Forecasting, 22, 981-1002, 10.1175/waf1033.1, 2007.

Chen, G., Zhao, K., Zhang, G., Huang, H., Liu, S., Wen, L., Yang, Z., Yang, Z., Xu, L., and Zhu, W.: Improving Polarimetric C-Band Radar Rainfall Estimation with Two-Dimensional Video Disdrometer Observations in Eastern China, Journal of Hydrometeorology, 18, 1375-1391, 10.1175/jhm-d-16-0215.1, 2017.

Chen, J.-M., Li, T., and Shih, C.-F.: Tropical Cyclone– and Monsoon-Induced Rainfall Variability in Taiwan, Journal of Climate, 23, 4107-4120, 10.1175/2010jcli3355.1, 2010.

Chen, J.-M., and Chen, H.-S.: Interdecadal Variability of Summer Rainfall in Taiwan Associated with Tropical Cyclones and Monsoon, Journal of Climate, 24, 5786-5798, 10.1175/2011jcli4043.1, 2011.

Chen, K., Chu, C.-Y., and Tzeng, Y.-C.: A semi-empirical model of rain attenuation at Ka-band in Northern Taiwan, Progress In Electromagnetics Research, 16, 213-223, 2011.

Chen, T.-C., Yen, M.-C., Hsieh, J.-C., and Arritt, R. W.: Diurnal and Seasonal Variations of the Rainfall Measured by the Automatic Rainfall and Meteorological Telemetry System in

https://doi.org/10.5194/hess-2020-345
Preprint. Discussion started: 21 August 2020


Hydrology and Earth System Sciences
Discussions

Taiwan, Bulletin of the American Meteorological Society, 80, 2299-2312, 10.1175/1520-0477(1999)080<2299:DASVOT>2.0.CO;2, 1999.

Chen, Y., Duan, J., An, J., and Liu, H.: Raindrop Size Distribution Characteristics for Tropical Cyclones and Meiyu-Baiu Fronts Impacting Tokyo, Japan, Atmosphere, 10, 391, 2019.

Chu, P.-S., Zhao, X., Lee, C.-T., and Lu, M.-M.: Climate prediction of tropical cyclone activity in the vicinity of Taiwan using the multivariate least absolute deviation regression method, Terrestrial Atmospheric and Oceanic Sciences, 18, 805, 2007.

Chu, Y.-H., and Su, C.-L.: An Investigation of the Slope–Shape Relation for Gamma Raindrop Size Distribution, Journal of Applied Meteorology and Climatology, 47, 2531-2544, 10.1175/2008jamc1755.1, 2008.

Dee, D. P., Uppala, S., Simmons, A., Berrisford, P., Poli, P., Kobayashi, S., Andrae, U., Balmaseda, M., Balsamo, G., and Bauer, d. P.: The ERA-Interim Reanalysis: Configuration and Performance of the Data Assimilation System, Quarterly Journal of the royal meteorological society, 137, 553-597, 2011.

Deo, A., and Walsh, K. J.: Contrasting tropical cyclone and non-tropical cyclone related rainfall drop size distribution at Darwin, Australia, Atmospheric Research, 181, 81-94, 2016.

Fornis, R. L., Vermeulen, H. R., and Nieuwenhuis, J. D.: Kinetic Energy–Rainfall Intensity Relationship For Central Cebu, Philippines for Soil Erosion Studies, Journal of Hydrology, 300, 20-32, 10.1016/j.jhydrol.2004.04.027, 2005.

Hu, Z., and Srivastava, R. C.: Evolution of Raindrop Size Distribution by Coalescence, Breakup, and Evaporation: Theory and Observations, Journal of the Atmospheric Sciences, 52, 1761-1783, 10.1175/1520-0469(1995)052<1761:EORSDB>2.0.CO;2, 1995.

Iguchi, T., Kozu, T., Meneghini, R., Awaka, J., and Okamoto, K. i.: Rain-Profiling Algorithm for the TRMM Precipitation Radar, Journal of Applied Meteorology, 39, 2038-2052, 10.1175/1520-0450(2001)040<2038:RPAFTT>2.0.CO;2, 2000.

Janapati, J., Seela, B. K., Lin, P.-L., Wang, P. K., and Kumar, U.: An assessment of tropical cyclones rainfall erosivity for taiwan, Scientific reports, 9, 15862, 2019.

Janapati, J., Seela, B. K., Lin, P.-L., Wang, P. K., Tseng, C.-H., Reddy, K. K., Hashiguchi, H., Feng, L., Das, S. K., and Unnikrishnan, C. K.: Raindrop Size Distribution Characteristics of Indian and Pacific Ocean Tropical Cyclones Observed at India and Taiwan Sites, Journal of the Meteorological Society of Japan. Ser. II, 98, 299-317, 10.2151/jmsj.2020-015, 2020.

Jayalakshmi, J., and Reddy, K. K.: Raindrop size distributions of southwest and northeast monsoon heavy precipitation observed over Kadapa (14°4′N, 78°82′E), a semi-arid region of India, Current Science, 107, 1312-1320, 2014.

Joss, J., and Waldvogel, A.: Raindrop Size Distribution and Sampling Size Errors, Journal of the Atmospheric Sciences, 26, 566-569, 10.1175/1520-0469(1969)026<0566:RSDASS>2.0.CO;2, 1969.

Jung, S.-A., Lee, D.-I., Jou, B. J.-D., and Uyeda, H.: Microphysical Properties of Maritime Squall Line Observed on June 2, 2008 in Taiwan, Journal of the Meteorological Society of Japan. Ser. II, 90, 833-850, 10.2151/jmsj.2012-516, 2012.

Kinnell, P. I. A.: Rainfall Intensity-Kinetic Energy Relationships for Soil Loss Prediction1, Soil Science Society of America Journal, 45, 153-155, 10.2136/sssaj1981.03615995004500010033x, 1981.

Krishna, U. V. M., Reddy, K. K., Seela, B. K., Shirooka, R., Lin, P.-L., and Pan, C.-J.: Raindrop size distribution of easterly and westerly monsoon precipitation observed over Palau

https://doi.org/10.5194/hess-2020-345
Preprint. Discussion started: 21 August 2020




islands in the Western Pacific Ocean, Atmospheric Research, 174-175, 41-51, https://doi.org/10.1016/j.atmosres.2016.01.013, 2016.

Kumar, S. B., and Reddy, K. K.: Rain drop size distribution characteristics of cyclonic and north east monsoon thunderstorm precipitating clouds observed over Kadapa (14.47°N, 78.82°E), tropical semi-arid region of India, Mausam, 64, 35–48, 2013.

Kumari, N., Kumar, S. B., Jayalakshmi, J., and Reddy, K. K.: Raindrop size distribution variations in JAL and NILAM cyclones induced precipitation observed over Kadapa (14.47 o N, 78.82 o E), a tropical semi-arid region of India, Indian Journal of Radio and Space Physics, 43, 57–66, 2014.

Kummerow, C., Hong, Y., Olson, W. S., Yang, S., Adler, R. F., McCollum, J., Ferraro, R., Petty, G., Shin, D. B., and Wilheit, T. T.: The Evolution of the Goddard Profiling Algorithm (GPROF) for Rainfall Estimation from Passive Microwave Sensors, Journal of Applied Meteorology, 40, 1801-1820, 10.1175/1520-0450(2001)040<1801:TEOTGP>2.0.CO;2, 2001.

Lee, M.-T., Lin, P.-L., Chang, W.-Y., Seela, B. K., and Janapati, J.: Microphysical Characteristics and Types of Precipitation for Different Seasons over North Taiwan, Journal of the Meteorological Society of Japan. Ser. II, 97, 841-865, 10.2151/jmsj.2019-048, 2019.

Liang, A., Oey, L., Huang, S., and Chou, S.: Long-term trends of typhoon-induced rainfall over Taiwan: In situ evidence of poleward shift of typhoons in western North Pacific in recent decades, Journal of Geophysical Research: Atmospheres, 122, 2750-2765, 10.1002/2017jd026446, 2017.

Liao, L., Meneghini, R., and Tokay, A.: Uncertainties of GPM DPR Rain Estimates Caused by DSD Parameterizations, Journal of Applied Meteorology and Climatology, 53, 2524-2537, 10.1175/JAMC-D-14-0003.1, 2014.

Lin, G.-W., and Chen, H.: The relationship of rainfall energy with landslides and sediment delivery, Engineering geology, 125, 108-118, 2012.

Lu, J.-Y., Su, C.-C., Lu, T.-F., and Maa, M.-M.: Number and volume raindrop size distributions in Taiwan, Hydrological Processes, 22, 2148-2158, 10.1002/hyp.6814, 2008.

Ma, Y., Ni, G., Chandra, C. V., Tian, F., and Chen, H.: Statistical characteristics of raindrop size distribution during rainy seasons in the Beijing urban area and implications for radar rainfall estimation, Hydrology and Earth System Sciences, 23, 4153-4170, 2019.

Maki, M., Keenan, T. D., Sasaki, Y., and Nakamura, K.: Characteristics of the Raindrop Size Distribution in Tropical Continental Squall Lines Observed in Darwin, Australia, Journal of Applied Meteorology, 40, 1393-1412, 10.1175/1520-0450(2001)040<1393:COTRSD>2.0.CO;2, 2001.

McFarquhar, G. M., Hsieh, T.-L., Freer, M., Mascio, J., and Jewett, B. F.: The characterization of ice hydrometeor gamma size distributions as volumes in N 0–λ–μ phase space: Implications for microphysical process modeling, Journal of the Atmospheric Sciences, 72, 892-909, 2015.

Nakajima, T., and King, M. D.: Determination of the Optical Thickness and Effective Particle Radius of Clouds from Reflected Solar Radiation Measurements. Part I: Theory, Journal of the Atmospheric Sciences, 47, 1878-1893, 10.1175/1520-0469(1990)047<1878:DOTOTA>2.0.CO;2, 1989.

Nakamura, K., and Iguchi, T.: Dual-wavelength Radar Algorithm, in: Measuring precipitation from space, Springer, 225-234, 2007.

https://doi.org/10.5194/hess-2020-345
Preprint. Discussion started: 21 August 2020


Hydrology and Earth System Sciences
Discussions

Platnick, S., King, M., and Hubanks, P.: MODIS Atmosphere L3 Daily Product, NASA MODIS Adaptive Processing System, Goddard Space Flight Center, in, 2015.

Radhakrishna, B., and Narayana Rao, T.: Differences in cyclonic raindrop size distribution from southwest to northeast monsoon season and from that of noncyclonic rain, Journal of Geophysical Research: Atmospheres, 115, 10.1029/2009jd013355, 2010.

Remer, L. A., Kaufman, Y. J., Tanré, D., Mattoo, S., Chu, D. A., Martins, J. V., Li, R. R., Ichoku, C., Levy, R. C., Kleidman, R. G., Eck, T. F., Vermote, E., and Holben, B. N.: The MODIS Aerosol Algorithm, Products, and Validation, Journal of the Atmospheric Sciences, 62, 947-973, 10.1175/JAS3385.1, 2005.

Renard, K. G., Foster, G. R., Weesies, G. A., McCool, D. K., and Yoder, D. C.: Predicting Soil Erosion byWater: A Guide to Conservation Planning with the Revised Universal Soil Loss Equation (RUSLE) (Agricultural Handbook 703). US Department of Agriculture, Washington, DC,, 1997.

Rosenfeld, D., and Ulbrich, C. W.: Cloud Microphysical Properties, Processes, and Rainfall Estimation Opportunities, Meteorological Monographs, 52, 237-258, 10.1175/0065-9401(2003)030<0237:CMPPAR>2.0.CO;2, 2003.

Ryzhkov, A. V., and Zrnić, D. S.: Comparison of Dual-Polarization Radar Estimators of Rain, Journal of Atmospheric and Oceanic Technology, 12, 249-256, 10.1175/1520-0426(1995)012<0249:CODPRE>2.0.CO;2, 1995.

Salles, C., Poesen, J., and Sempere-Torres, D.: Kinetic Energy of Rain and Its Functional Relationship With Intensity, Journal of Hydrology, 257, 256-270, 10.1016/S0022-1694(01)00555-8, 2002.

Seela, B. K., Janapati, J., Lin, P.-L., Reddy, K. K., Shirooka, R., and Wang, P. K.: A Comparison Study of Summer Season Raindrop Size Distribution Between Palau and Taiwan, Two Islands in Western Pacific, Journal of Geophysical Research: Atmospheres, 122, 11,787-711,805, 10.1002/2017jd026816, 2017.

Seela, B. K., Janapati, J., Lin, P.-L., Wang, P. K., and Lee, M.-T.: Raindrop Size Distribution Characteristics of Summer and Winter Season Rainfall Over North Taiwan, Journal of Geophysical Research: Atmospheres, 123, 11,602-611,624, 10.1029/2018jd028307, 2018.

Steiner, M., Smith, J. A., and Uijlenhoet, R.: A Microphysical Interpretation of Radar Reflectivity–Rain Rate Relationships, Journal of the Atmospheric Sciences, 61, 1114-1131, 10.1175/1520-0469(2004)061<1114:Amiorr>2.0.Co;2, 2004.

Testud, J., Oury, S., Black, R. A., Amayenc, P., and Dou, X.: The Concept of "Normalized" Distribution to Describe Raindrop Spectra: A Tool for Cloud Physics and Cloud Remote Sensing, Journal of Applied Meteorology, 40, 1118-1140, 10.1175/1520-0450(2001)040<1118:TCONDT>2.0.CO;2, 2001.

Thompson, E. J., Rutledge, S. A., Dolan, B., and Thurai, M.: Drop Size Distributions and Radar Observations of Convective and Stratiform Rain over the Equatorial Indian and West Pacific Oceans, Journal of the Atmospheric Sciences, 72, 4091-4125, 10.1175/JAS-D-14-0206.1, 2015.

Tokay, A., and Short, D. A.: Evidence from Tropical Raindrop Spectra of the Origin of Rain from Stratiform versus Convective Clouds, Journal of Applied Meteorology, 35, 355-371, 10.1175/1520-0450(1996)035<0355:Eftrso>2.0.Co;2, 1996.

https://doi.org/10.5194/hess-2020-345
Preprint. Discussion started: 21 August 2020



Tokay, A., Kruger, A., and Krajewski, W. F.: Comparison of Drop Size Distribution Measurements by Impact and Optical Disdrometers, Journal of Applied Meteorology, 40, 2083-2097, 10.1175/1520-0450(2001)040<2083:CODSDM>2.0.CO;2, 2001.

Tokay, A., Bashor, P. G., Habib, E., and Kasparis, T.: Raindrop Size Distribution Measurements in Tropical Cyclones, Monthly Weather Review, 136, 1669-1685, 10.1175/2007mwr2122.1, 2008.

Tu, J.-Y., and Chou, C.: Changes in precipitation frequency and intensity in the vicinity of Taiwan: typhoon versus non-typhoon events, Environmental Research Letters, 8, 014023, 10.1088/1748-9326/8/1/014023, 2013.

Ulbrich, C. W., and Atlas, D.: Microphysics of Raindrop Size Spectra: Tropical Continental and Maritime Storms, Journal of Applied Meteorology and Climatology, 46, 1777-1791, 10.1175/2007JAMC1649.1, 2007.

van Dijk, A. I. J. M., Bruijnzeel, L. A., and Rosewell, C. J.: Rainfall Intensity–Kinetic Energy Relationships: A Critical Literature Appraisal, Journal of Hydrology, 261, 1-23, 10.1016/S0022-1694(02)00020-3, 2002.

Wen, L., Zhao, K., Chen, G., Wang, M., Zhou, B., Huang, H., Hu, D., Lee, W.-C., and Hu, H.: Drop size distribution characteristics of seven typhoons in China, J. Geophys. Res. Atmos., 123, 6529–6548, doi:10.1029/2017JD027950, 2018.

Wen, L., Zhao, K., Wang, M., and Zhang, G.: Seasonal Variations of Observed Raindrop Size Distribution in East China, Advances in Atmospheric Sciences, 36, 346-362, 2019.

Wischmeier, W. H.: A Rainfall Erosion Index for a Universal Soil-Loss Equation1, Soil Science Society of America Journal, 23, 246-249, 10.2136/sssaj1959.03615995002300030027x, 1959.

Wu, Z., Zhang, Y., Zhang, L., Lei, H., Xie, Y., Wen, L., and Yang, J.: Characteristics of summer season raindrop size distribution in three typical regions of western Pacific, Journal of Geophysical Research: Atmospheres, 124, 4054-4073, 2019.

Zhang, Y., Liu, L., Bi, S., Wu, Z., Shen, P., Ao, Z., Chen, C., and Zhang, Y.: Analysis of dual-polarimetric radar variables and quantitative precipitation estimators for landfall typhoons and squall lines based on disdrometer data in southern China, Atmosphere, 10, 30, 2019.

https://doi.org/10.5194/hess-2020-345
Preprint. Discussion started: 21 August 2020


Hydrology and Earth System Sciences
Open Access
EGU
Discussions

**Table 1.** Rainy minutes (N), mean, standard deviation (Std), Skewness and Kurtosis of seven rainfall rate classes for typhoon (TY) and non-typhoon (NTY) rainy days of summer seasons.

| Rain rate class | Rain rate threshold | Typhoon (TY) | | | | | non-typhoon (NTY) | | | | |
|---|---|---|---|---|---|---|---|---|---|---|---|
| | | No. of samples | Mean ( mm $h^{-1}$) | Standard deviation (mm $h^{-1}$) | Skewness | Kurtosis | No. of samples | Mean ( mm $h^{-1}$) | Standard deviation (mm $h^{-1}$) | Skewness | Kurtosis |
| C1 | $0.1 \leq R < 1$ | 9317 | 0.43 | 0.26 | 0.55 | 2.1 | 10661 | 0.4 | 0.25 | 0.71 | 2.34 |
| C2 | $1 \leq R < 2$ | 3274 | 1.44 | 0.29 | 0.24 | 1.84 | 3193 | 1.43 | 0.29 | 0.29 | 1.88 |
| C3 | $2 \leq R < 5$ | 4747 | 3.29 | 0.85 | 0.31 | 1.92 | 3404 | 3.17 | 0.83 | 0.46 | 2.1 |
| C4 | $5 \leq R < 10$ | 2799 | 7 | 1.4 | 0.43 | 2.04 | 1404 | 6.98 | 1.42 | 0.43 | 2.01 |
| C5 | $10 \leq R < 30$ | 2313 | 16.44 | 5.24 | 0.77 | 2.59 | 1234 | 17.46 | 5.6 | 0.5 | 2.08 |
| C6 | $30 \leq R < 50$ | 393 | 38.31 | 5.73 | 0.37 | 1.92 | 320 | 37.88 | 5.67 | 0.45 | 2.01 |
| C7 | $R > 50$ | 231 | 67.15 | 14.91 | 1.16 | 3.97 | 152 | 65.86 | 14.94 | 1.51 | 5.18 |
| total | | 23074 | 4.88 | 9.38 | 4.59 | 31.51 | 20368 | 3.59 | 8.38 | 5.2 | 38.9 |

https://doi.org/10.5194/hess-2020-345
Preprint. Discussion started: 21 August 2020


Hydrology and Earth System Sciences
Open Access
Discussions

**Table 2.** Statistical parameters [correlation coefficient: $R^2$, Root mean square error (RMSE), normalized RMSE] for typhoon (TY) and non-typhoon (NTY) rainy days.

| Weather system | Statistical parameter | $KE_{time}$–$R$ | | $KE_{mm}$–$R$ | | | $KE_{mm}$–$D_m$ |
|---|---|---|---|---|---|---|---|
| | | Linear | Power | Power | Exp | Log | Second order polynomial |
| TY | $R^2$ | 0.986 | 0.994 | 0.694 | 0.68 | 0.68 | 0.992 |
| | RMSE | 37.488 | 24.785 | 3.973 | 10.227 | 4.047 | 12.396 |
| | NRMSE | 0.306 | 0.202 | 0.032 | 0.083 | 0.033 | 2.514 |
| NTY | $R^2$ | 0.984 | 0.99 | 0.646 | 0.639 | 0.639 | 0.988 |
| | RMSE | 38.012 | 30.745 | 4.599 | 11.017 | 4.636 | 12.93 |
| | NRMSE | 0.322 | 0.26 | 0.039 | 0.093 | 0.039 | 2.803 |

https://doi.org/10.5194/hess-2020-345
Preprint. Discussion started: 21 August 2020

Hydrology and Earth System Sciences
Discussions

# Figures

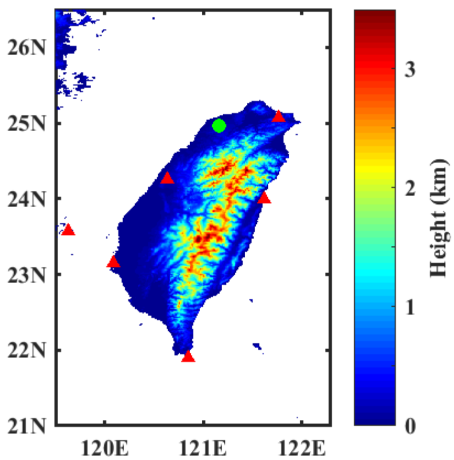


**Figure 1.** Taiwan geography with the location of disdrometer (green color circle) and radars (red color triangles).

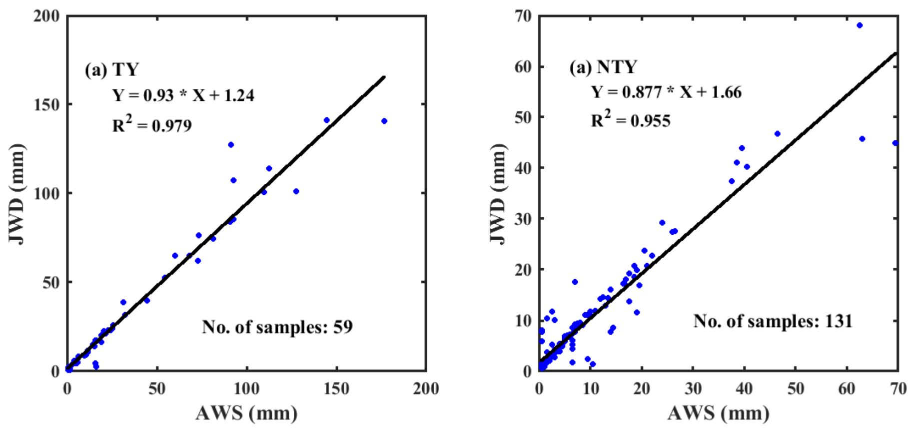


**Figure 2**. Comparison JWD measured daily accumulated rainfall amounts with the collocated rain gauge for (a) typhoon (TY) and (b) non-typhoon (NTY) rainy days of summer seasons.

https://doi.org/10.5194/hess-2020-345
Preprint. Discussion started: 21 August 2020




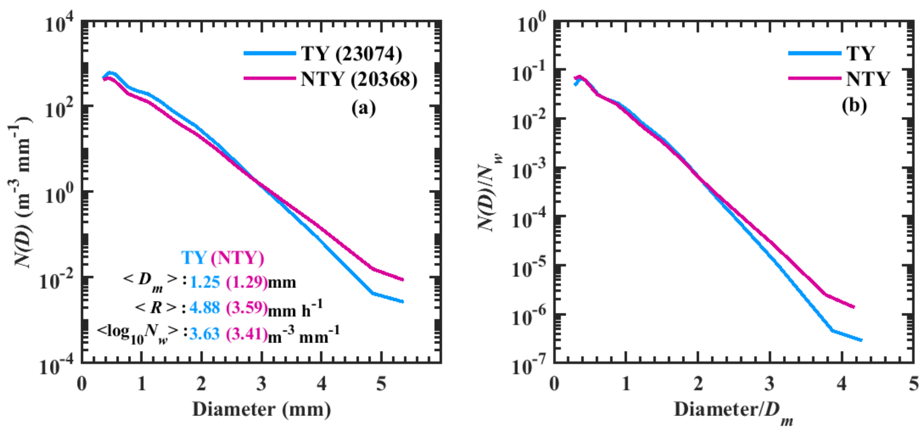


**Figure 3**. (a) Distributions of mean concentration [*N(D)*, in mm$^{-1}$ m$^{-3}$] with raindrop diameter for typhoon (TY) and non-typhoon (NTY) rainfall and their (b) normalized spectra.

https://doi.org/10.5194/hess-2020-345
Preprint. Discussion started: 21 August 2020


Hydrology and Earth System Sciences
Discussions

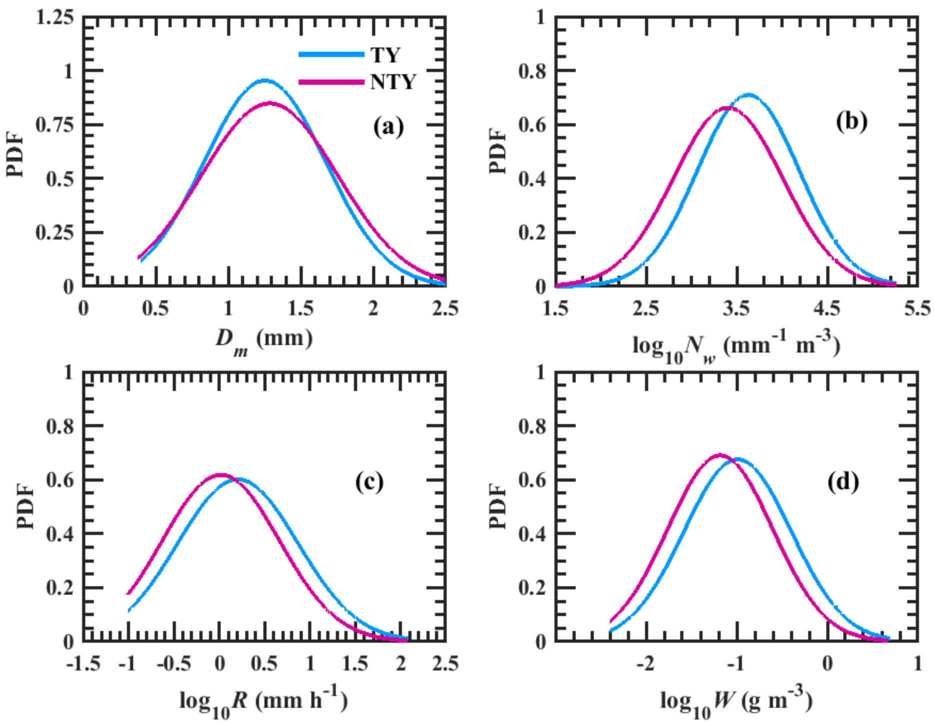


**Figure 4.** (a) mass-weighted mean diameter, $D_m$ (mm), (b) $\log_{10}N_w$, where $N_w$ is the normalized intercept parameter (mm$^{-1}$ m$^{-3}$) (c) $\log_{10}R$, where $R$ is rainfall rate (mm h$^{-1}$) (d) $\log_{10}W$, where $W$ is liquid water content (g m$^{-3}$) probability distribution functions (PDF) for typhoon (TY) and non-typhoon (NTY) rainy days of summer seasons.

https://doi.org/10.5194/hess-2020-345
Preprint. Discussion started: 21 August 2020



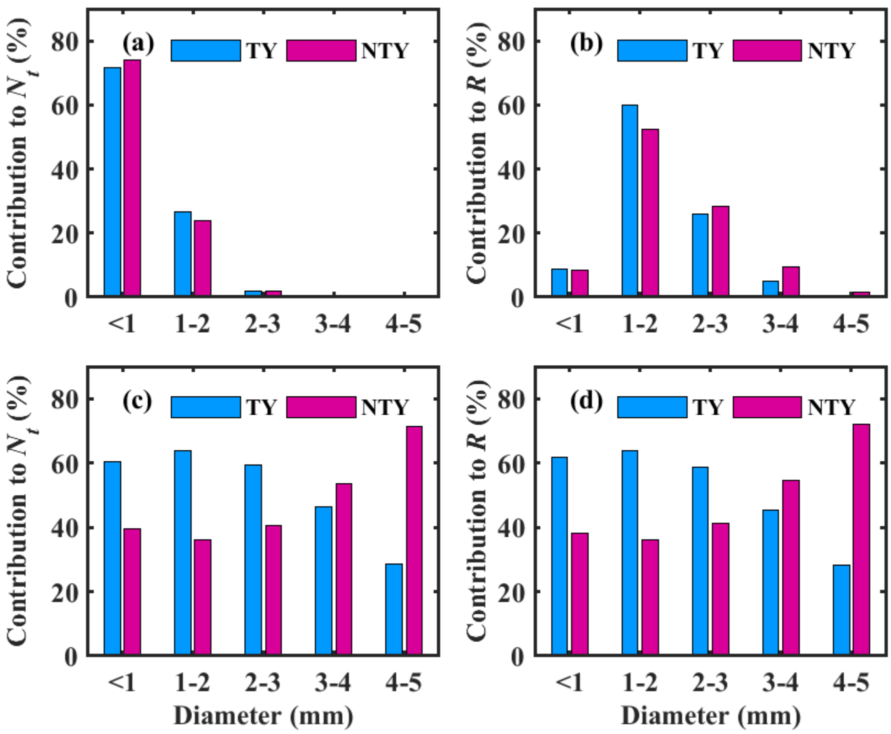


**Figure 5.** Contribution of drop diameter classes (Diameter < 1 mm, 1−2 mm, 2−3 mm, 3−4 mm, and 4−5 mm) to (a) total number concentration $N_t$ ($m^{-3}$) and (b) rainfall rate $R$ (mm $h^{-1}$) in typhoon (TY) and non-typhoon (NTY) rainfall of summer seasons. Percentage of typhoon (TY) and non-typhoon (NTY) rainfall in each diameter class for (c) total number concentration $N_t$ ($m^{-3}$) and (d) rainfall rate $R$ (mm $h^{-1}$).

https://doi.org/10.5194/hess-2020-345
Preprint. Discussion started: 21 August 2020

Hydrology and Earth System Sciences
Discussions

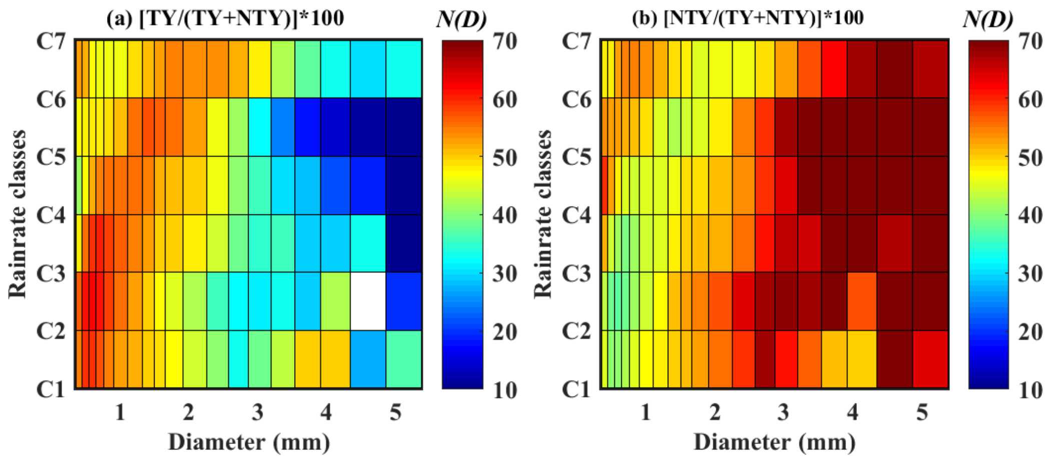


**Figure 6** Percentage contribution of raindrop concentration [$N(D)$, mm$^{-1}$ m$^{-3}$] in different rainfall rate ranges for typhoon (TY) and non-typhoon (NTY) rainfall of summer seasons.

https://doi.org/10.5194/hess-2020-345
Preprint. Discussion started: 21 August 2020


Hydrology and Earth System Sciences
Discussions

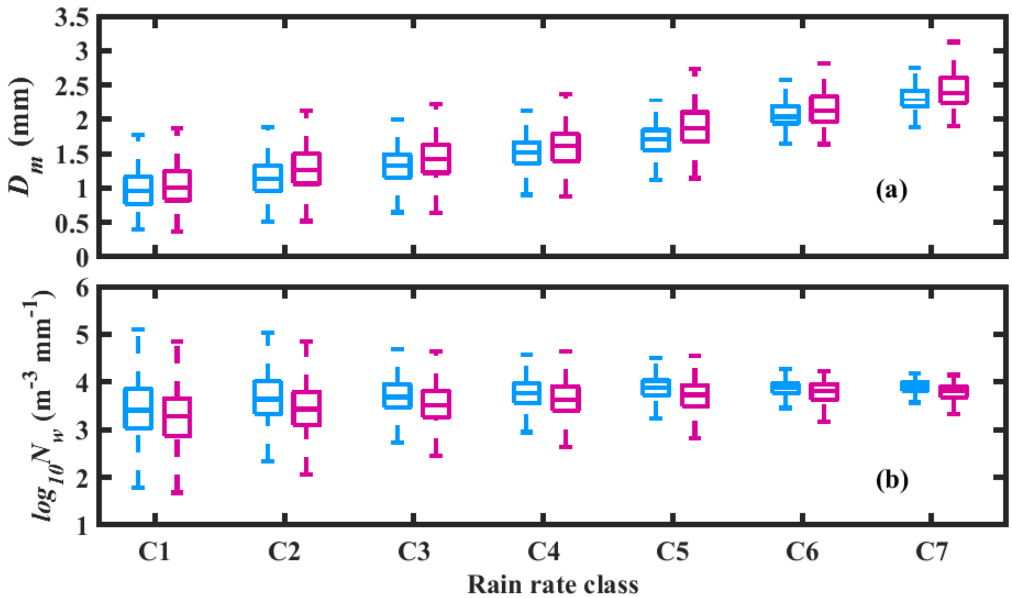


**Figure 7.** Box plot of (a) $D_m$ (mm) and (b) $\log_{10}N_w$ ($mm^{-1}$ $m^{-3}$) in seven rainfall rate intervals for typhoon (TY) (sky blue color) and non-typhoon (NTY) (dark magenta color) rainfall. The center line of the box indicates the median, and the bottom and top lines of the box indicate the 25th and 75th percentiles, respectively. The bottom and top of the dashed vertical lines indicate the 5th and 95th percentiles, respectively.

https://doi.org/10.5194/hess-2020-345
Preprint. Discussion started: 21 August 2020


Hydrology and Earth System Sciences
Discussions
Open Access

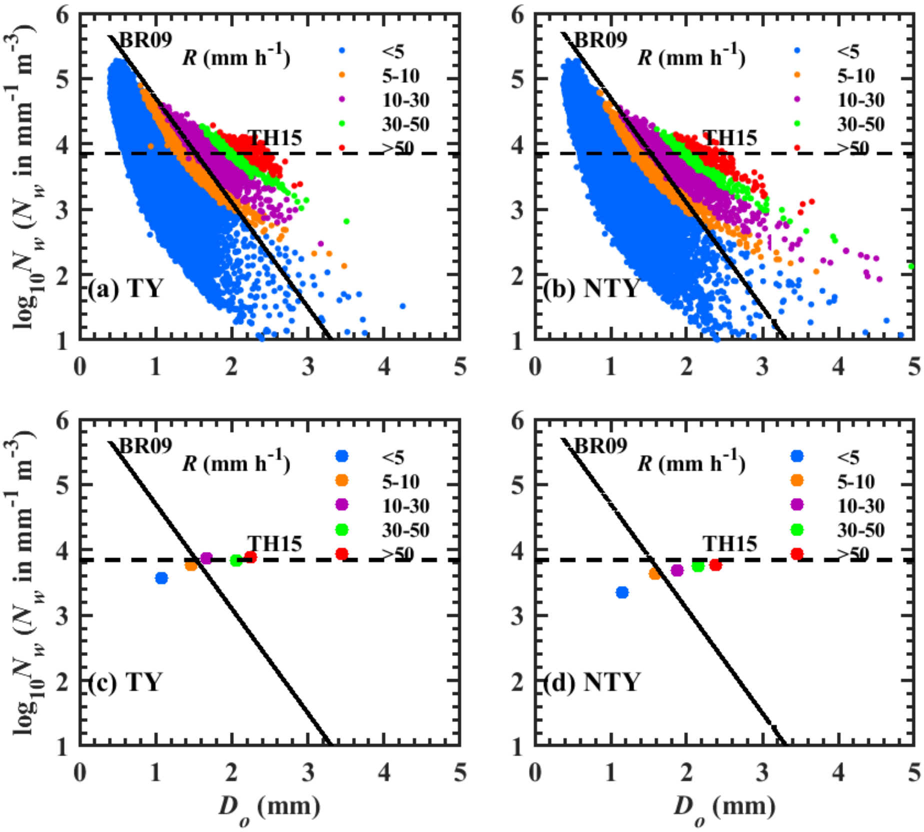


**Figure 8.** Scatter plots of $D_0$-$\log_{10}N_w$ for (a) typhoon (TY) and (b) non-typhoon (NTY) rainfall in different rainfall rate ranges. Mean values of $D_0$ and $\log_{10}N_w$ for (c) typhoon (TY) and (d) non-typhoon (NTY) rainfall in different rainfall rate ranges. Stratiform and convective regimes separation line of Thompson et al. (2015): TH15 and Bringi et al. (2009): BR09 are represented with horizontal dotted line and inclined solid line, respectively.

https://doi.org/10.5194/hess-2020-345
Preprint. Discussion started: 21 August 2020




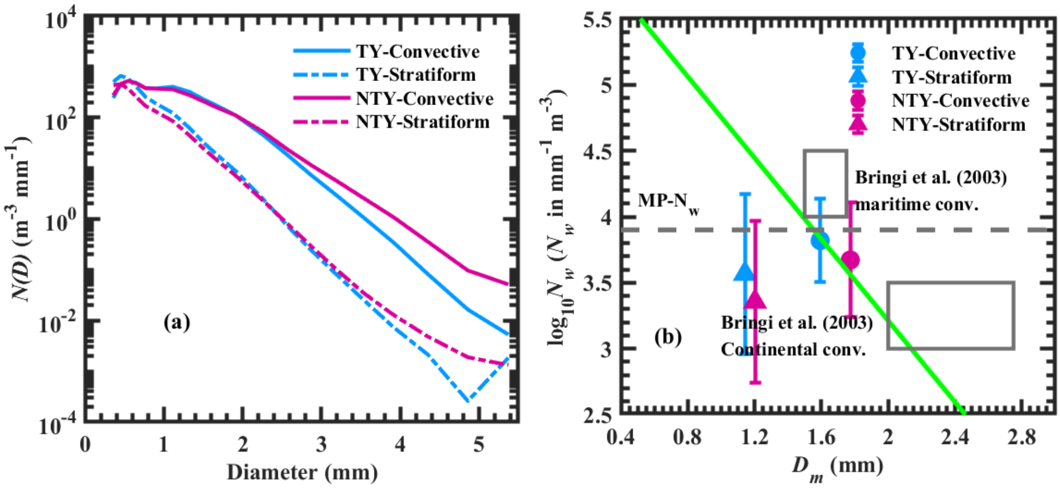


**Figure 9**. (a) Distribution of $N(D)$ ($m^{-3}$ $mm^{-1}$) with raindrop diameter in stratiform and convective regimes for typhoon (TY) and non-typhoon (NTY) rainfall. (b) Variations of $\log_{10}N_w$ (where $N_w$ is the normalized intercept parameter in $mm^{-1}$ $m^{-3}$) with $D_m$ (mass-weighted mean diameter in mm) values in stratiform and convective regimes for typhoon (TY) and non-typhoon (NTY) rainfall. The horizontal gray dashed line is the Marshall-Palmer value of $\log_{10}N_w$ (3.9) for exponential shape. The green dash dotted line is the stratiform and convective separation line of Bring et al. (2003).

https://doi.org/10.5194/hess-2020-345
Preprint. Discussion started: 21 August 2020


Hydrology and Earth System Sciences
Open Access
Discussions

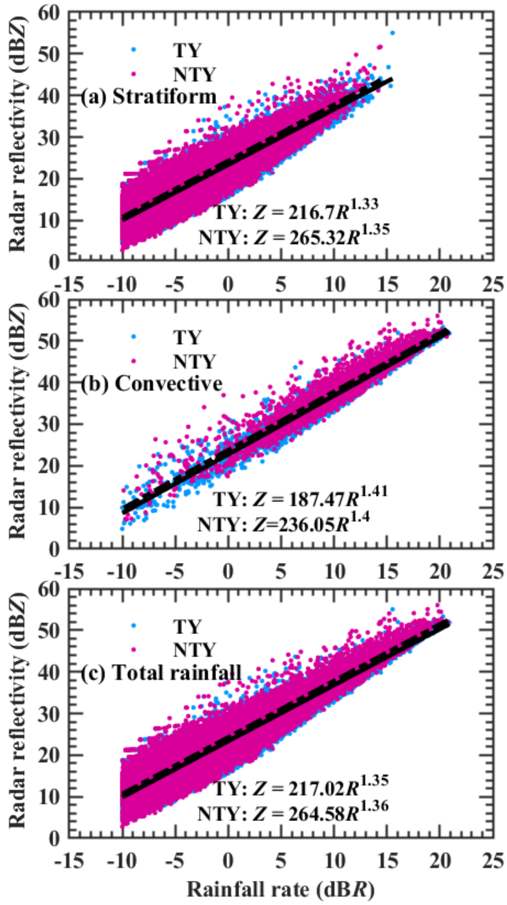


**Figure 10.** Scatter plots of radar reflectivity ($Z$, dB$Z$) and logarithmic scale of rainfall rate ($10*\log_{10}R$, dB$R$, $R$ in mm $h^{-1}$) for typhoon (TY) and non-typhoon (NTY) rainfall.

https://doi.org/10.5194/hess-2020-345
Preprint. Discussion started: 21 August 2020



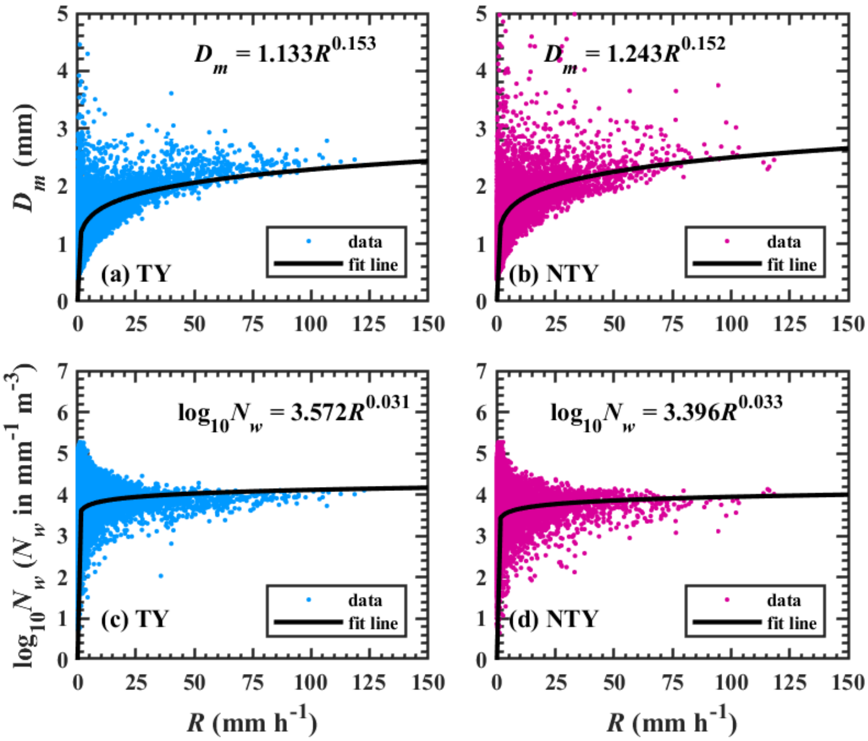


**Figure 11.** Distributions of $D_m$ (mm) and $\log_{10}N_w$ $N_w$ in mm$^{-1}$ m$^{-3}$) with rainfall rate ($R$, mm h$^{-1}$) for typhoon (TY) and non-typhoon (NTY) rainy days of summer seasons.

.

https://doi.org/10.5194/hess-2020-345
Preprint. Discussion started: 21 August 2020



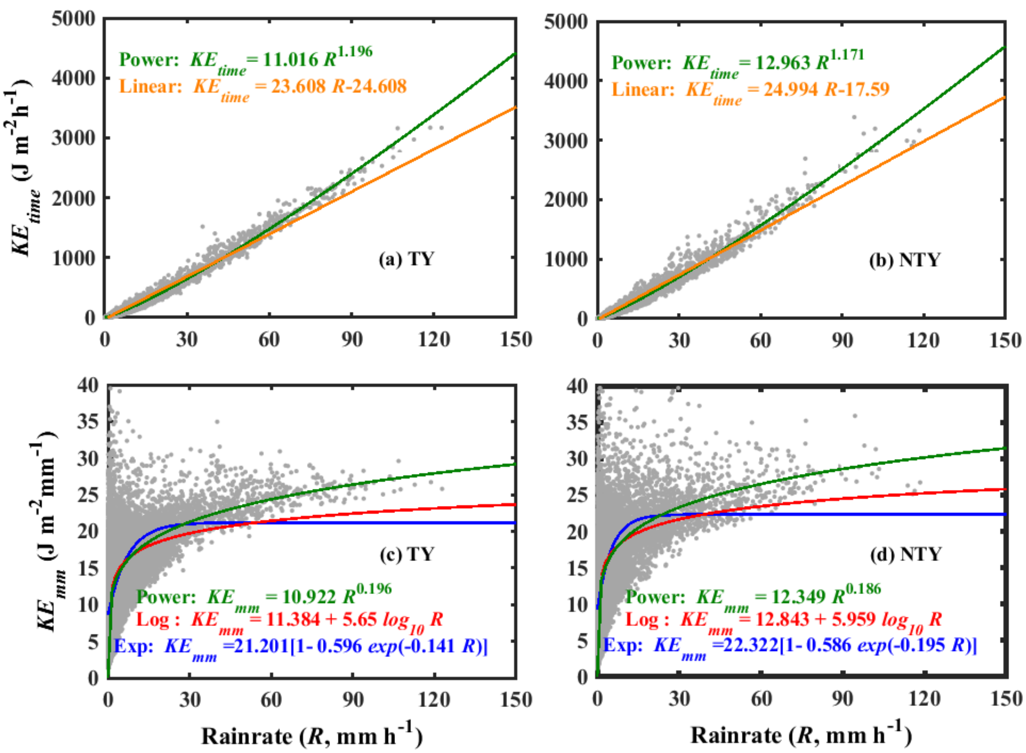


**Figure 12.** Scatter plots of rainfall kinetic energy (*KE*) [time-specific *KE*, $KE_{time}$; volume-specific *KE*, $KE_{mm}$] with rainfall rate (*R*, mm $h^{-1}$) for typhoon (TY) and non-typhoon (NTY) rainy days of summer seasons.

https://doi.org/10.5194/hess-2020-345
Preprint. Discussion started: 21 August 2020



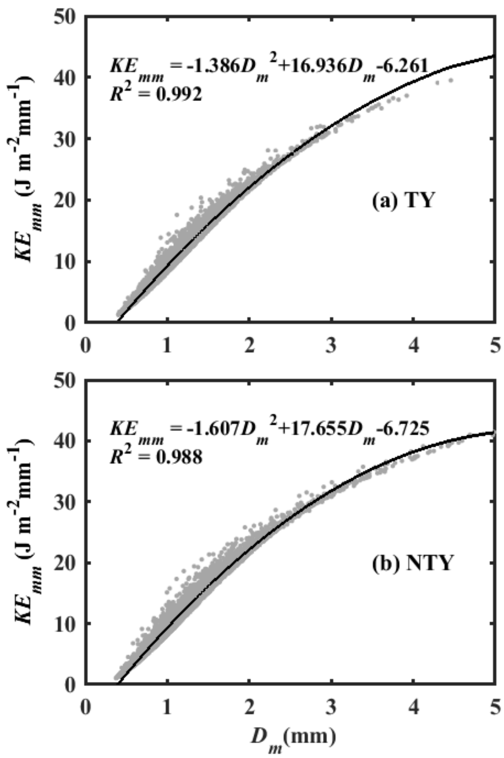


**Figure 13.** Scatter plots of volume-specific *KE* (*$KE_{mm}$* in J m$^{-2}$ mm$^{-1}$] with $D_m$ (mm) for typhoon (TY) and non-typhoon (NTY) rainy days of summer seasons.

https://doi.org/10.5194/hess-2020-345
Preprint. Discussion started: 21 August 2020

Hydrology and Earth System Sciences
Open Access
Discussions

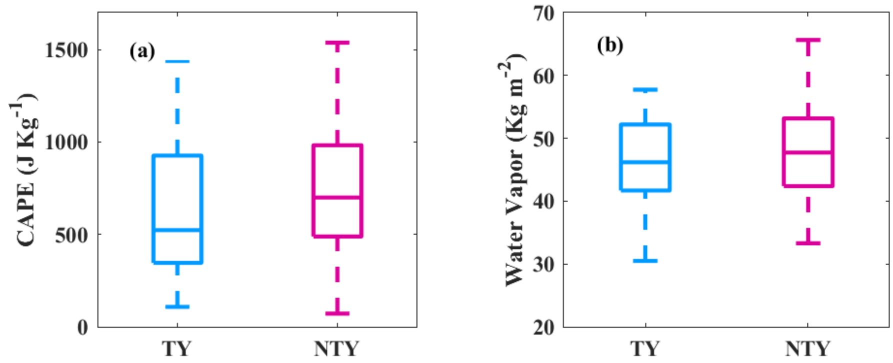


**Figure 14:** Variations in (a) convective available potential energy (CAPE, J Kg$^{-1}$) and (b) vertical integral of water vapor (kg m$^{-2}$) for typhoon (TY) and non-typhoon (NTY) rainy days of summer seasons over disdrometer observational site. The center line of the box indicates the median, and the bottom and top lines of the box indicate the 25$^{th}$ and 75$^{th}$ percentiles, respectively. The bottom and top of the dashed vertical lines indicate the 5$^{th}$ and 95$^{th}$ percentiles, respectively

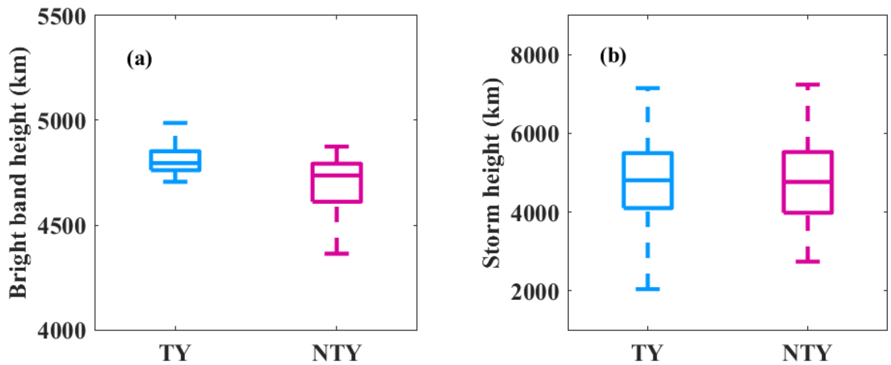


**Figure 15.** (a) bright band (BB) and storm heights box plots for typhoon (TY) and non-typhoon (NTY) rainy days of summer seasons over disdrometer observational site.

https://doi.org/10.5194/hess-2020-345
Preprint. Discussion started: 21 August 2020

Hydrology and Earth System Sciences
Discussions

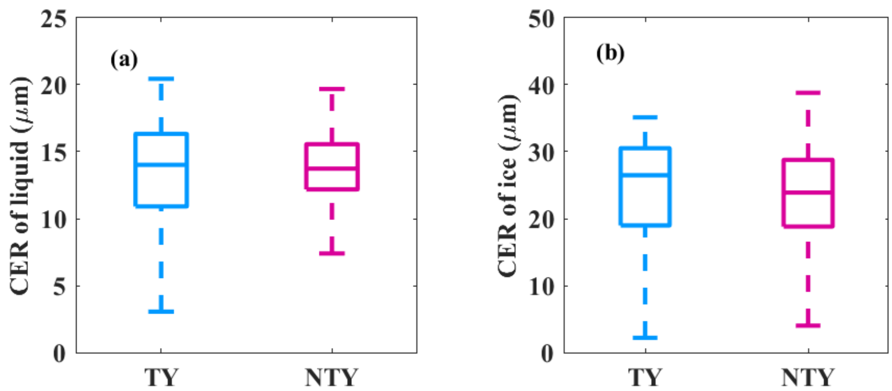


**Figure 16.** (a) liquid, (b) ice particles cloud effective radii (CER, μm) values for typhoon (TY) and non-typhoon (NTY) rainy days of summer seasons over disdrometer observational site.

https://doi.org/10.5194/hess-2020-345
Preprint. Discussion started: 21 August 2020


Hydrology and Earth System Sciences
Discussions

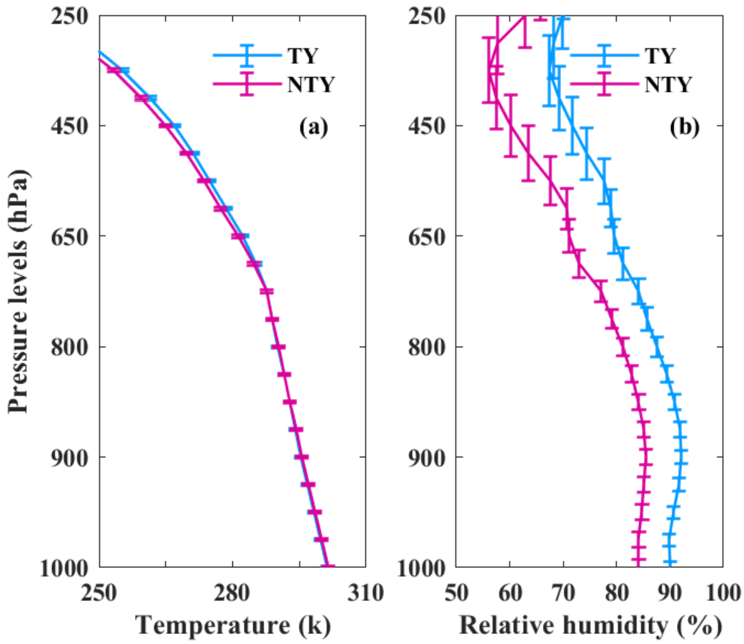


776

777 **Figure 17.** Mean air temperature ($^{o}$C) and relative humidity (%) profiles for typhoon (TY) and

778 non-typhoon (NTY) rainy days of summer seasons over the disdrometer observational

779 site.

780

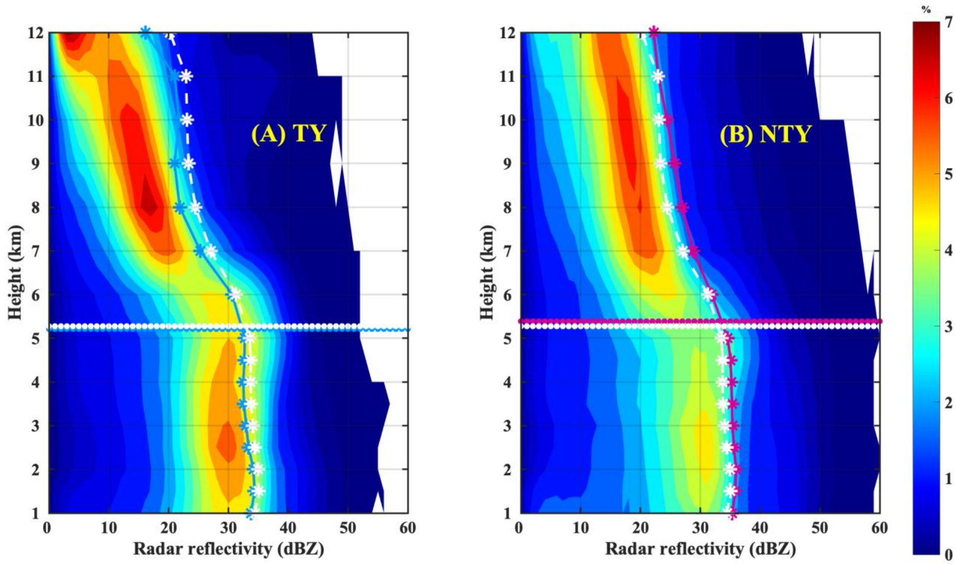


**Figure 18.** Contoured frequency-by-altitude diagram of radar reflectivity from six ground-based radars for (a) typhoon (TY) and (b) non-typhoon (NTY) rainy days of summer seasons.

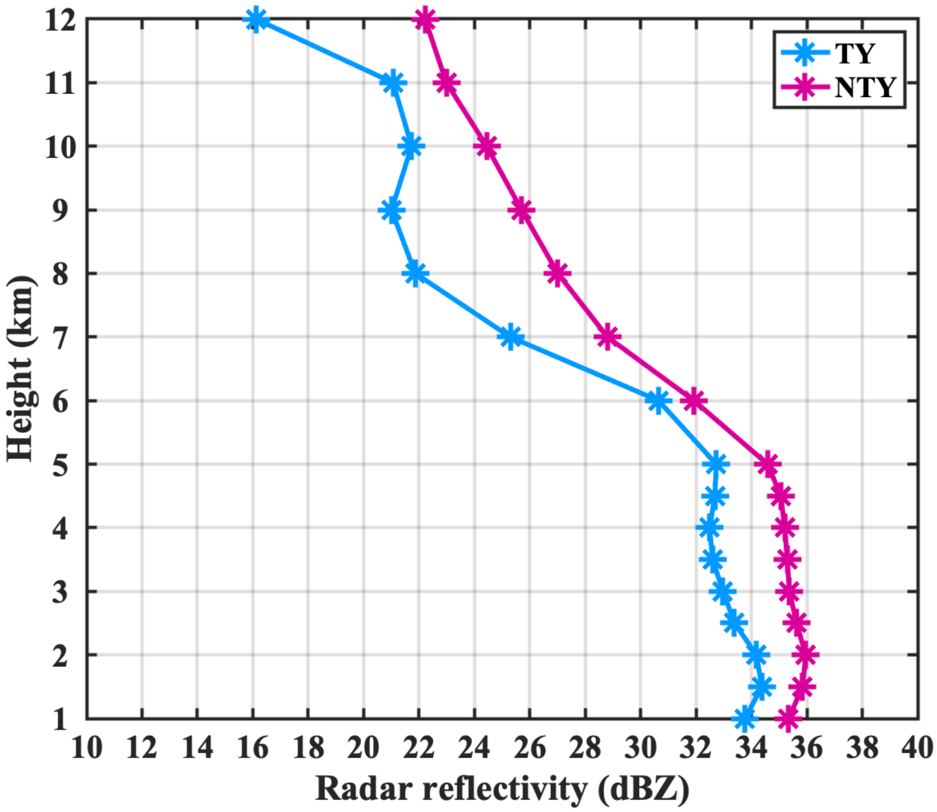


**Figure 19.** Mean radar reflectivity profiles of typhoon (TY) and non-typhoon (NTY) rainy days of summer seasons over the disdrometer observational site.